OCEAN AND ATMOSPHERE TELECONNECTIONS MODULATE EAST TROPICAL PACIFIC PRODUCTIVITY AT LATE TO MIDDLE PLEISTOCENE TERMINATIONS

Paula Diz[1]*, Ivan Hernández-Almeida[2], Patricia Bernárdez[1], Marta Pérez-Arlucea[1], Ian R. Hall[3]

[1]Dept. Marine Geosciences, Faculty of Sciences, University of Vigo, 36310, Spain
[2]Geological Institute, Department of Earth Science, ETH, 8092, Zürich, Switzerland
[3]School of Earth and Ocean Sciences, Cardiff University, CF10 3AT, U.K.

* Corresponding author, pauladiz@uvigo.es

Abstract

The modern Eastern Equatorial Pacific (EEP) is a key oceanographic region for regulating the Earth´s climate system, accounting for between 5–10% of global marine production whilst also representing a major source of carbon dioxide efflux to the atmosphere. Changes in ocean dynamics linked to the nutrient supply from the Southern Ocean have been suggested to have played a dominant role in regulating EEP productivity over glacial–interglacial timescales of the past 500 ka. Yet, the full extent of the climate and oceanic teleconnections and the mechanisms promoting the observed increase of productivity occurring at glacial terminations remain poorly understood. Here we present multi-proxy, micropaleontological, geochemical and sedimentological records from the easternmost EEP to infer changes in atmospheric patterns and oceanic processes potentially influencing regional primary productivity over glacial-interglacial cycles of the mid-late Pleistocene (~0-650 ka). These proxy data support a leading role for the north-south migration of the Intertropical Convergence Zone (ITCZ) in shaping past productivity variability in the EEP. Productivity increases during glacial periods and notably peaks at major and "extra" glacial terminations (those occurring 1-2 precession cycles after some major terminations) coincident with the inferred southernmost position of the ITCZ. The comparison of our reconstructions with proxy records of climate variability suggests the intensification of related extratropical atmospheric and oceanic teleconnections during deglaciation events. These processes may have re-activated the supply of southern sourced nutrientsto the EEP, potentially contributing to enhanced productivity in the EEP and thus counterbalancing the oceanic carbon dioxide outgassing at glacial terminations.

KEYWORDS:

East Equatorial Pacific, Intertropical Convergence Zone, benthic foraminifera, paleoproductivity, teleconnections, Pleistocene terminations.

HIGHLIGHTS

- New multi-proxy record from the East Equatorial Pacific for the last 650 ka
- ITCZ latitudinal shifts drove productivity changes
- Ocean tunnelling likely contributed to increased productivityat terminations
- Tropical atmospheric changes key in deglaciations
- EEP contributes to the deglacial atmospheric carbon dioxide regulation

1. Introduction

The modern East Equatorial Pacific (EEP) plays an important role in climate regulation as it is an important source of carbon dioxide (CO_2) to the atmosphere (Takahashi et al., 2009). Yet, it accounts for 5-10% of the global oceanic primary production while comprising only 9% of the ocean area (Pennington et al., 2006). Nutrients and CO_2-rich waters are currently supplied to the EEP thermocline via Subantarctic Mode Water(Sarmiento et al., 2003). Modern biogeochemical models suggest that Subantarctic Mode Waterprovides a substantial fraction (30-50%) of the nutrients that reach the EEP, thereby sustaining a large proportion of the export production in this area (Palter et al., 2010). However, the mechanisms driving glacial to interglacial changes in the biological productivity and export production in the EEP remain equivocal. The supply of micronutrients (i.e., iron) have long been proposed as one of the main influences on the efficiency and strength of the oceanic biological pump in the past (e.g. Murray et al., 2012). Yet, a recent study have argued that variability in the atmospheric dust input (a major source of iron) to the EEP was not large enough to trigger a substantial increase in glacial productivity and that nutrient supply from the Southern Ocean might have played a crucial role in controlling the equatorial Pacific productivity over the Late Pleistocene (Winckler et al., 2016). The south to equatorial connection, through so called “oceanic

tunnelling" (Spero and Lea, 2002) appears to have been active in the past, in particular during the last deglaciation (Martinez-Boti et al., 2015) and likely during older deglaciations (Rippert et al., 2017). However, little is known about the functioning of the oceanic tunnelling during other mid-late Pleistocene terminations and its influence on the biological pump in the EEP and therefore global climate.

Furthermore, the EEP is involved ininterhemispheric thermal and moisture transport through changes in the mean position and strength of the Hadley circulation cells, which are intimately linked to the meridional position of the Intertropical Convergence Zone (ITCZ) (Schneider et al., 2014). Changes in the average position of the ITCZ are relevant not only at a global scale, controlling global atmospheric reorganizations (Chiang et al., 2014), but also regionally, involving changes in the position of oceanographic structures such as the Costa Rica Dome (CRD). The CRD is an open-ocean upwelling system in the EEP that develops seasonally off the coast of Central America (Fiedler, 2002). It has been previously suggested that past changes in the intensity and location of the CRD upwelling system depends on the intensity of the trade winds linked to the meridional position of the ITCZ (Hofmann et al., 1981), and that such variability could influence regional productivity patterns in the EEP duringthe last glacial cycle (Ivanova et al., 2012). It is unclear to what extent atmospheric processes (e.g., ITCZ-related CRD variability), in addition to oceanic processes (e.g., ocean tunnelling), might have influenced past productivity patterns in the EEP during the mid to late Pleistocene.

Here we present a multi-proxy record to investigate the mechanisms controlling past variability in productivity in the EEP at glacial-interglacial time scales. The record is obtained from the Integrated Ocean Drilling Program (IODP), Expedition 344, Site U1381 (Hole U1381C) located off the Costa Rica margin (Figure 1). The core site is ideally located to capture signals related to the past changes in the EEP productivity which might

101 have occurred either through variations in the position of the ITCZ, which controls the
102 extension and location of the CRD, and/or through fluctuations in the nutrient supply from
103 southern sourced waters. Accordingly, we use proxies providing information for the
104 quantity and quality of the organic carbon supply to the seafloor (e.g., benthic
105 foraminiferal faunal composition, planktonic foraminiferal abundance, organic carbon and
106 opal content) and sediment chemical composition (e.g., calcium carbonate and major
107 elemental content). These multi-proxy derived records allow us to investigate the
108 mechanisms controlling past variability in productivity and make inferences on the
109 contribution of atmospheric and oceanicprocesses at the glacial terminations throughout
110 the Middle to Late Pleistocene (the last 650 ka).
111
112 **2. Core location and oceanography**

113 The Hole U1381C (08°25.7027′N; 84°09.48′W, Harris et al., 2013, Figure 1) is located
114 ~4.5 km offshore the Osa Peninsula, on the Costa Rica margin at the southern end of the
115 East Pacific Warm Pool (Fiedler and Talley, 2006). The core site was recovered at 2065
116 meters, well above the depth of the modern sedimentary lysocline, which is established at
117 ~ 2900 meters water depth for the Panama basin (Thunell et al., 1981). At present, primary
118 production in surface waters at Site U1381 is relatively low as its location is not directly
119 influenced by the seasonal (wind-driven) upwelling or the current position of the open
120 ocean upwelling center of the CRD (Figure 1a-b) . The lack of seasonal coastal (wind-
121 driven) upwelling at our site is because of the proximity to the Talamanca mountains
122 (3000-4000 m height) which favour the convergence of local wind curl patterns
123 (Pennington et al., 2006). This contrasts with the seasonal coastal upwelling processes
124 occurring south (Gulf of Panama, Panamá) and north (Gulf of Papagayo, Nicaragua) of the
125 Site U1381 (Figure 1c-d). The CRD is a “permanent” anticlinal thermal structure flowing

126 cyclonically and is currently centred around 9ºN and 90ºW with a diameter ranging
127 between 100 to 900 km (Figure 1a-b). The CRD position and magnitude is related to the
128 seasonal migration of the ITCZ and associated wind stress curl patterns, and can be
129 identified by shallowing of the thermocline, which corresponds to the isotherm of 20°C
130 (Fig. 1a-b).
131
132 **3. Material and methods**
133 *3.1. Sediment samples*
134 Sediment samples from Site U1381 (Hole U1381C) were obtained during IODP
135 Expedition 344 (Harris et al., 2013). We analysed the uppermost 47 mcored depth scale
136 (CSF-B, meters below sea floor, mbsf, from U1381C 344-1H-1W 0-2 cm to 344-6H-1W
137 89-91 cm)which is characterised by a monotonous sequence of light greenish gray
138 hemipelagic silty clay (Harris et al., 2013). Two cm thick sediment samples for faunal
139 analysis samples (~10 cm^3) were collected at a 10 cm spacing for the upper 20 mbsf and in
140 20 cm intervals for 20-47 mbsf. Samples for geochemical analysis (2 cm thick, ~10 cm^3)
141 were typically taken immediately below intervals sampled for faunal analysis.
142
143 *3.2. Stable isotope analysis and age model development*
144 The age model of Hole U1381C is constructed by the combination of radiocarbon dates, a
145 planktonic biostratigraphic event and graphical correlation of the the benthic oxygen
146 isotopic ($\delta^{18}O$) record from Hole U1381C to the LR04 benthic foraminiferal $\delta^{18}O$ stack
147 (Lisiecki and Raymo, 2005). The age control of the upper sections (4.3 mbsf) is
148 constrained by seven accelerator mass spectrometry ^{14}C ages on planktonic foraminifera
149 from the >150 μm (mixed species or monospecific depending on the availability of
150 individuals weighing between ~2 to 10 mg; see Supplementary Information S.I.1). The

151 accelerator mass spectrometry ages were measured at the Center for Applied Isotope
152 Studies, University of Georgia (U.S.A.) and were calibrated (2σ confidence limits) with
153 the Calib 7.0 software using the Marine13 calibration dataset (Reimer et al., 2013). The
154 oldest radiocarbon age was too old for calibration and was discarded for the age model
155 construction. The last occurrence of the planktonic foraminifera *Globigerinoides ruber*
156 (pink variety) occurring at 8.95 mbsf which corresponds to an age of ~127 ka (Ivanova et
157 al., 2012), was also used as a dating point (See supplementary information S.I.1). Beyond
158 the radiocarbon limits, the U1381C benthic $\delta^{18}O$ was correlated graphically to the orbitally
159 tuned LR04 benthic $\delta^{18}O$ stack record using the AnalySeries program. For this purpose, 3-
160 4 visually clean individuals of *Uvigerina auberiana* d´Orbigny were selected per sample
161 from the 250-300 μm size fraction. Stable isotope analyses were performed on a
162 ThermoFinnigan MAT 253 mass spectrometer coupled to a Kiel IV carbonate preparation
163 device at Cardiff University (UK). The spectrometer was calibrated through the
164 international standard NBS-19, and all isotopic results are reported as a per mil deviation
165 from the Vienna Pee Dee Belemnite scale (‰ VPDB). The reproducibility of the $\delta^{18}O$
166 analyses is ±0.05%, based on replicate measurements of carbonate standards. According
167 to our age model, the studied interval covers the last ~650 ka. Average sedimentation rates
168 are 6.7 cm ka^{-1}, ranging from very low values of ~ 1.6 cm ka^{-1}during Marine Isotope Stage
169 (MIS) 2, MIS 4 and MIS 14 (which remain poorly resolved in our record) to high values of
170 ~ 9 cm ka^{-1} from MIS 5 through MIS 11 (See Supplementary Figure S1). The mean
171 temporal resolution of the records is 2 ka.
172
173 *3.3. Foraminiferal faunal analyses*
174 Benthic foraminiferal assemblages provide information about the quality, quantity and
175 sustainability of the organic carbon flux to the seafloor as well as oxygenation conditions

176 in the sediment and bottom waters (Gooday, 2003). Samples for benthic foraminifera
177 analyses were dried at 45ºC, weighed and sieved to 63 μm, and then weighed again after
178 drying. The weight percent of the >63 μm fraction was calculated from dried samples (%
179 coarse fraction, CF). To investigate benthic foraminiferal assemblages, a representative
180 split of at least ~ 200 individuals (when possible) from the > 125 μm fraction was
181 indentified and counted and the relative abundance (percentage) of the characteristic
182 species calculated. The abundance of benthic foraminifera (BF) was calculated from the
183 number of individuals counted in the split (or the whole sample when the abundance was
184 low) per gram of total dry weight sediment (number of benthic foraminifera >125 μm /g).
185 While a detailed analysis of the benthic foraminiferal fauna assemblage is out of the scope
186 of this study, ecological information is provided for the most characteristic species, or
187 group of species, relevant for a broad interpretation of paleoenvironmental conditions. In
188 order to describe the patterns of planktonic foraminifera abundance along the core, a split
189 of whole planktonic foraminifera from the >150 μm size fraction was counted and used to
190 calculate the abundance of planktonic individuals per gram of dry weight sediment
191 (number of planktonic foraminifera >150 μm /g).

192 *3.4. Organic and inorganic carbon, total nitrogen and opal contents*

193 Total bulk sediment samples for organic carbon and nitrogen content were dried at 45°C,
194 ground and homogenized using a zircon ball mill. The total weight percent of sedimentary
195 carbon (% C) and nitrogen (% N), as well as inorganic carbon (% C_{inorg}) and organic
196 carbon (% C_{org}) were measured using a macro elemental analyzer LECO CNS2000 at
197 CACTI (University of Vigo). The % C and % N measurements were calibrated against a
198 standard reference material (Ethylenediaminetetraacetic acid-EDTA and pure $CaCO_3$). The
199 detection limit was 0.02 % for % C and 0.01 % for % N, respectively, while repeat
200 analyses (n = 5) of the standards yielded precisions of ± 0.14 for % C and ± 0.3 % N

201 respectively. For the estimation of $\%C_{inorg}$ an aliquot of the homogenized sample was
202 heated at 450ºC for 3 hours to remove organic carbon. The total weight percent of calcium
203 carbonate (% $CaCO_3$) was calculated as 8.33 x % C_{inorg}. The % C_{org} content was calculated
204 as the difference between % C and % C_{inorg}.

205 The concentration of sedimentary biogenic silica (i.e., % opal) is considered as a proxy for
206 siliceous export production (Anderson et al., 2009). Opal abundance was determined using
207 the method of Mortlock and Froelich (1989). The precision and accuracy of opal analysis
208 were monitored using replication of an in-house standard. The coefficient of variability
209 (e.g. standard deviation) is ± 0.2 %. The Si_{opal}/C_{org} (hereinafter Si/C) were calculated after
210 transformation of the biogenic silica (opal) and % C_{org} into molar ratios. The Si/C ratios are
211 used here as a proxy for the contribution of siliceous producers to non-siliceous primary
212 producers (Ragueneau et al., 2000).
213 Sedimentary mass accumulation rates are provided for geochemical and sedimentological
214 tracers to complement the information provided by relative abundance values. Mass
215 accumulation rates are calculated as the weight percentage of sedimentary component x
216 dry bulk density (g cm^{-3}) x linear sedimentation rates (cm ka^{-1}). Linear sedimentation rates
217 are calculated from the tie points obtained for the construction of the age model
218 (Supplementary Table S1). Dry bulk density values are from Harris et al. (2013). Mass
219 accumulation rates range from 1 to 9 g cm^{-2} ka^{-1} and are within the range previously
220 estimated for the Panama basin (Kienast et al., 2007).
221
222 *3.5. Sediment chemical elements*
223 Sediment composition and provenance was evaluated by the quantification of elemental
224 concentrations of major elements (Ca, Ti, Al). For the analysis of chemical elements, dried
225 and ground sediments were prepared on pressed pellets and measured by X-ray

Fluorescence (XRF) using Mo as the X-ray source on a Siemens SRS 3000 spectrometer at CACTI (University of Vigo). Reference samples (NRC MESS-3 and NRC PACS-2) were analyzed and used as routine quality control samples, to assess the instrument accuracy and to obtain quantitative values. Quantification was done using the Spectraplus Software through the EVAL program by k-factor of proximity of reference samples. Replicate measurements (n = 5) show good agreement between certified and analytical values. Recovery was in general over 87% for MESS-3, whereas for PACS-2 it was nearly 100% for all the studied elements. The typical absolute error for each element determination is lower than 5%. The Ti was normalized to the Al content, an indicator of the aluminosilicate fraction of the sediments. The Ti (unlike Fe) is less sensitive to environmental redox variations and it is used here as a terrigenous proxy (Tribovillard et al., 2006).The Ca content was normalized to Ti (Ca/Ti) and it is used here as an indirect proxy for the carbonated versus terrigenous fraction of the sediment.

4. Results

4.1.-Calcium carbonate related proxies

As the Hole U1381C is ~850 m above the regional carbonate saturation horizon in the Panama Basin (Thunell et al., 1981) it is not expected to have experienced severe carbonate dissolution (López-Otálvaro et al., 2008). However, previous studies in the area have identified some episodes of carbonate dissolution during the last glacial cycle (Ivanova et al., 2012). In order to interpret the $CaCO_3$variability at the core site and to assess whether carbonate dissolution influenced the composition of benthic foraminiferal assemblages, we used several independent proxies for $CaCO_3$ dissolution and $CaCO_3$production (e.g., LaMontagne et al., 1996): % $CaCO_3$ and mass accumulation of $CaCO_3$, major elemental ratios (Ca/Ti), % >63 μm coarse fraction, relative abundance of

benthic to planktonic plus benthic foraminifera (B/P+B), % C_{org}, and the absolute abundances of benthic and planktonic foraminifera (number of BF or PF/g) (Figure 2b-f). The$CaCO_3$record (% and mass accumulation) of Hole U1381C shows high values during glacial periods (5-15%) and low values during interglacials (<5%) (Figure 2b). The % $CaCO_3$ concentrations (and indirect proxies for sedimentary $CaCO_3$ content such as Ca/Ti) peaks at major and so-called "extra terminations" (i.e., terminations exhibiting patterns of events similar to main terminations, but occurring 1-2 precession cycles before), such as Termination IIIa (TIIIa, between MIS 7c and 7d) and Termination VIIa (TVIIa, between MIS 15a and 15b) (Cheng et al., 2016). Paleoproductivity related proxies; % C_{org}, abundance of planktonic and benthic foraminifera and % >63 μm (which is mainly composed by planktonic and benthic foraminifera with occasional skeletons of diatoms and radiolaria) exhibit generally high values during glacial periods and terminations and low values during interglacial periods (Figure 2 c-f). The observed trends are statistically supported by positive correlations (see Supplementary Table S.I.2). The relationship between parameters seems to be noticeable at major and extra terminations, where there is a significant correspondence with peaks in % $CaCO_3$ (and indirect proxies i.e., Ca/Ti, Figure 2b), % >63μm fraction (Figure 2c) benthic foraminifera absolute abundance (Figure 2d) and % C_{org} (Figure 2f). Benthic foraminifera generally outnumber planktonic foraminifera (B/P+B> 0.5, Figure 2e) except for glacial stages, terminations and sub-stages.

4.2.-Geochemical proxies.

The %C_{org} ranges from 0.2 to 2.2% (mean 1.9%) and concentrations increase at glacial periods and peak at terminations (Figure 2f). The C_{org}/N values range from 4.4 to 13 (mean=9, see supplementary data), suggesting that the C_{org} at the core site is mainly of marine provenance (Meyers, 1997). In contrast to %C_{org}, the % opal, which varies between

7% and 11%, shows only minor glacial-interglacial variability, (Figure 2g), but a clear decrease in % opal at terminations. The Si/C, a proxy for the abundance of siliceous to non-siliceous primary producers, shows higher values during interglacials than during glacials, with the lowest values occurring at terminations (Figure 3g). The record of Ti/Al, a proxy for the terrigenous provenance of the sediments, varies between 0.05 and 0.09 (Figure 3h). This variability range is comparable to other published Ti/Al records used to infer terrigenous influence in marine sediments (e.g., Yarincik et al., 2000, Figure 3i). The values of Ti/Al in the core U1381C show anincreasing trend from interglacials to terminations when ratios show the highest values (Figure 3h).

4.3.- Benthic foraminifera assemblages

The abundance of benthic foraminifera increases during glacial periods and peaks at terminations (Figure 3a-b). Interglacial periods are characterized by low foraminiferal numbers and the dominance of *Uvigerina peregrina* (Cushman) and *Uvigerina auberiana* (d´Orbigny) together showing abundances higher than 40 % (Figure 3c) and therefore grouped under the so-called "*Uvigerina* spp.". This contrasts with the abundance pattern of *Cassidulina carinata* Silvestri (Figure 3e) and secondary species *Valvulineria glabra* Cushman and *Rotamorphina laevigata* (Phleger and Parker) (Figure 3f). *Cassidulina carinata* almost disappears from the assemblage during interglacials (0-5%) but shows increased concentrations and percentages (10-30%) during glacials and terminations. A similar glacial-interglacial pattern is shown by *V. grabra* and *R. laevigata*. The last deglacial period is characterized by a different set of species to the other terminations (Figure 3d). *Bolivina interjuncta* Cushman, *Bolivina seminuda* (Cushman), *Bolivina* cf. *plicata* d´Orbigny, *Epistominella pacifica* (Cushman), and *Epistominella smithi* (Steward and Steward) characterize the assemblage of the last termination.

5. Discussion

5.1. The carbonate record of Hole U1381C

The factors explaining EEP $CaCO_3$ variability are still under debate (Winckler et al., 2016) with some studies suggesting that $CaCO_3$ productivity is the main driver (Lyle et al., 2002) and others instead proposing deep water carbonate chemistry (Sexton and Barker, 2012). Separating the signals of production anddissolution in $CaCO_3$ related proxies is difficult because both influences might have acted either concurrently or differently over time. It therefore requires the use of several independent proxies for both $CaCO_3$ production and dissolution (see section 4.1). The overall correlation between % $CaCO_3$ and indirect proxies for paleoproductivity (% Corg, absolute abundance of benthic and planktonic foraminifera) suggests that $CaCO_3$ production played a prime role in shaping sedimentary $CaCO_3$ content at our EEP Site (Figure 2b-d). The strong correspondence between peaks of % $CaCO_3$ and foraminiferal absolute abundance suggests that $CaCO_3$ production, rather than minimum dissolution (preservation), is also the most likely cause for $CaCO_3$ deglacial peaks at the core site. As an exception to this general relationship is a period of moderate dissolution identified between ~ 20 and 110 ka. This interval is characterized by high B/P+B ratios (Figure 2e) and planktonic assemblages dominated by dissolution resistant species, such as *Globorotalia menardii* (see Supplementary Information, Figure S2). Intense dissolution intervals are identified around the transition between maximum interglacial and glacial declines of MIS 11 and MIS 5 (Figure 2; brown bars). These intervals are represented by the extremely low abundance of whole shells of planktonic foraminifera, low numbers of benthic foraminifera, low mass accumulation rate of the coarse fraction, and depressed % $CaCO_3$ content. These samples might be affected by dissolution and paleoenvironmental interpretation has been considered with caution.

Inferred peaks of organic export and $CaCO_3$ production occur at all seven major glacial terminations (except for Termination V) and the "extra terminations". Notably, the $CaCO_3$ accumulation and benthic foraminiferal abundance peaks exhibit comparable values at both major and extra terminations (including terminations occurring during the period of mild interglacials MIS13 and MIS15). The pattern described by our records at Termination V differs from the other terminations in that the high % $CaCO_3$ values do not occur at the termination but rather during mid glacial MIS 12 (Figure 2a-b, f).

5.2. Paleoproductivity from benthic foraminifera: the influence of the CRD

As outlined above, the productivity proxies at Site U1381C (e.g., C_{org} and benthic foraminiferal abundance) at Site U1381C typically exhibit high values during glacial periods and terminations and low values during interglacial periods (Figure 2a, d-f, Figure 3a-b). The deglacial productivity maxima are consistent with results from other studies in the EEP for the last deglaciation (Ivanova et al., 2012) and older terminations (Winckler et al., 2016). Benthic foraminiferal assemblages can provide additional information about the potential mechanisms involved in those paleoproductivity changes over the last 650 ka. The group *Uvigerina* ssp. occurs in higher relative abundances during interglacial periods (Figure 3c). One of the species within the group, *Uvigerina auberiana* is an infaunal species considered well adapted to high fluxes of organic carbon under perennial upwelling regimes and low to moderate oxygenation environments (e.g., Licari and Mackensen, 2005). Similar ecological preferences are considered for *U. peregrina*, for which some studies also indicate its preference for refractory organic material (Morigi et al., 2001). Therefore, high relative abundance of *Uvigerina* spp. during interglacials is suggested to indicate relatively high to moderate, but sustained organic carbon flux to the seafloor. At the same time, glacial periods and terminations (TII-TVII) are characterized by higher benthic foraminifera abundances and increased numbers of *Cassidulina carinata* and

350 secondary species *Valvulineria glabra* and *Rotamorphina laevigata* (Figure 3e,f).
351 Ecological studies indicate that *C. carinata* favours the seasonal delivery of food to the
352 seafloor occurring during phytoplankton bloom events (Goineau et al., 2011) and that the
353 species of the genus *Valvulineria* (*V. bradyana*, *V. mexicana*) prefer eutrophic conditions
354 (Mojtahid et al., 2010). This allows for the interpretation of the occurrence of *C. carinata*
355 (and secondary species) as an indicator of the seasonal delivery of fresh and abundant
356 organic carbon to the seafloor (likely from phytoplankton blooms) in an overall context of
357 high productivity during glacials and terminations. This suggests that glacial-interglacial
358 changes in productivity are related to a variable influence of organic carbon supply from a
359 seasonal versus permanent source. There are at least two potential sources to consider that
360 which might have driven the seasonal productivity changes at Hole U1381C: (i) coastal
361 upwelling and (ii) the CRD upwelling system. Coastal (wind-driven) upwelling is not
362 favoured at the core site because of proximal high mountain ranges (See description of
363 core location and oceanography in Section 2); therefore, the most plausible source of a
364 seasonally variable organic carbon supply to Site U1381, during glacial periods and their
365 terminations, is the seasonal CRD open-ocean upwelling system. Thus, interglacial
366 conditions characterized by species related to sustainable organic carbon flux to the
367 seafloor, are interpreted as prevailing during a weak influence of the CRD over the study
368 site (similarly to the present conditions) in contrast to glacials and terminations, which are
369 interpreted as occurring when the influence of the CRD over the core site is at its highest
370 and the organic carbon input to the seafloor occurs seasonally. The similar composition of
371 modern benthic foraminiferal assemblages, as those described above, under the influence
372 of the CRD (9-11ºN;Heinz et al., 2008) and outside its influence (4-8ºN; Betancur and
373 Martinez, 2003) supports our interpretation. Recent foraminiferal assemblages under the
374 influence of the CRD show increased abundances of *Cassidulina carinata* (Heinz et al.,

375 2008) in comparison with assemblages from areas not directly affected by (or outside) the
376 influence of this open ocean upwelling system, which are dominated by *Uvigerina* species
377 (Betancur and Martinez, 2003). Following the arguments discussed above, we suggest
378 using the abundance of *Uvigerina* spp. group as an indirect proxy for the relative influence
379 of the CRD at Hole U1381C, with increased (decreased) abundance of these species being
380 related to distal (proximal) influence of the CRD (Figure 3c).

381 The suggestion of increased influence of the CRD over the core site during glacials and
382 terminations is also consistent with the record of sedimentary Si/C ratios (Figure 3g). The
383 CRD is a unique open ocean upwelling system as, in contrast to other upwelling systems
384 where productivity is dominated by large size diatoms, productivity is governed by
385 cyanobacteria of the *Synechococus* group (Krause et al., 2016 and references therein).
386 Consequently, the contribution of diatoms to the organic matter export is low (Krause et
387 al., 2016). Therefore, low sedimentary Si/C ratios are expected when the CRD is close to
388 the Site U1381. Indeed, Si/C ratios are low during glacials and reach their lowest values
389 coincident with terminations (Figure 3g) further supporting the interpretation of changes in
390 the position of the CRD based on the benthic foraminiferal assemblages.

391 The foraminiferal assemblages characterizing the last deglacial period and the early
392 Holocene suggest the occurrence of intermediate to strong oxygen depletion in the bottom
393 waters, based on the known tolerance of *Bolivina interjuncta, Bolivina seminuda, Bolivina*
394 cf. *plicata* and *Epistominella smithi* and *E. pacifica* for hypoxic conditions (Silva et al.,
395 1996) (Figure 3e). Intermediate hypoxic conditions in the bottom waters are likely the
396 result of a combination of physical (i.e., reduced oxygen ocean solubility, water
397 stratification and warming) and biological processes (Tetard et al., 2017 and references
398 therein) including the excess of organic carbon supply to the sea floor delivered from
399 enhanced productivity under the influence of the CRD. The latter is supported by low Si/C

ratios. A similar hypoxic deglacial event has been also described in areas to the north of our location such as Baja California and Santa Barbara basin (Tetard et al., 2017).

5.3.-Atmospheric control on the local oceanography

In the modern ocean, the trajectory of the CRD varies seasonally with the position of the ITCZ (Fiedler, 2002, Figure 1). Thus, change in the CRD position to be more (less) frequently over the site during glacial intervals and terminations (interglacials) requires a southward (northward, similar to nowadays) shift in the relative position of the ITCZ. Additionally, a northern (southern) position of the ITCZ would lead to increased (decreased) precipitation in the EEP(Chiang et al., 2014). Hence, an increased influence of the CRD over our site should parallel evidence for decreased precipitation and fluvial input. The influence of freshwater inputs to Site U1381 can be assessed from the relative influence of the detrital signal recorded in the elemental ratios Ti/Al (Figure 3h). The variations in the Ti/Al ratios are interpreted to be driven by changes in the terrestrial run off with low (high) ratios indicating more (less) run off (Yarincik et al., 2000). There is an overall clear relation between low relative abundance of the *Uvigerina* spp. group interpreted as increased influence of the CRD over the site (southern position of the ITCZ), with high Ti/Al values indicating low terrestrial runoff. This correspondence, together with other available proxies for the migration of the ITCZ in the tropical Atlantic (i.e., Ti/Al record from the Cariaco Basin (Figure 3i, Yarincik et al., 2000), strongly supports the suggestion that Hole U1381C is primarily recording the relative position of the ITCZ and its influence on the regional hydrography of the EEP. This interpretation is further supported by the similarity of the U1381C Ti/Al record and foraminiferal patterns during

terminations to the $\Delta\delta^{18}O$ record from Chinese speleothems (Figure 4e). The speleothem $\delta^{18}O$ record is interpreted to represent abrupt changes in the precipitation regime in Central Asia related to the seasonal shifts in the ITCZ position that influences the strength of the Asian Monsoon (Cheng et al., 2016). When the ITCZ is displaced northward (southward) the northern hemisphere summer monsoon strengthens (weakens), increasing precipitation and yielding lower (higher) speleothem $\delta^{18}O$ values (higher $\Delta\delta^{18}O$, Figure 4e). The correspondence between the southernmost position on the ITCZ recorded in U1381C and the weakening of the Asian monsoon supports previous suggestions that such ITCZ shifts are coherent over long distances (Schneider et al., 2014). Notably, our data extends previous inferences from marine records (Jacobel et al., 2016) for the southward migration of the ITCZ during the last two glacial terminations, indicating that comparable latitudinal ITCZ variability likely characterised earlier terminations as well, such as TIV, TV, TVI, TVII and the extra terminations TIIIa, TVIIa. This finding reinforces the idea that tropical atmospheric changes play an essential role in the deglaciation process (Denton et al., 2010).

5.4.- Potential contribution of extra-tropical waters to EEP productivity during terminations

The deglacial productivity maxima observed at U1381C are related to the southward migration of the ITCZ. This tropical atmospheric shift is relevant for interhemispheric oceanic and atmospheric connectivity, which play a role in the increase of productivity at terminations in the EEP. Thus, the inferred southward shifts in the ITCZ are coincident (within age model uncertainties of ~ 4ka) with evidence for the delivery of ice-rafted debris (IRD) to the high latitude North Atlantic sediments (Figure 4f), an indirect proxy for perturbations in the Atlantic Meridional Overturning Circulation (e.g., Barker et al., 2015). This linkage can be explained by atmospheric teleconnections which are reproduced in

449 coupled ocean-atmosphere models showing that large reductions in the Atlantic Meridional
450 Overturning Circulation can induce a southward shift in the ITCZ over the Pacific (Chiang
451 et al., 2014). Climate models indicate that a southward migration of the ITCZ during
452 Atlantic Meridional Overturning slowdown in the Northern Hemisphere could also cause a
453 southward shift and intensification of the Southern Hemisphere westerlies (Ceppi et al.,
454 2013). A southward displacement of the southern hemisphere westerlies would have
455 contributed to warming the Southern Ocean and Antarctica (Denton et al., 2010). Besides,
456 a weak mode of the Atlantic Meridional Overturning Circulation triggers a heat transport
457 to the Southern Hemisphere, also warming the Southern Ocean and Antarctic continent via
458 the thermal bipolar seesaw (Stocker and Johnsen, 2003). Ocean warming (i.e., retrieval of
459 glacial ice) and the shift in the Southern Ocean wind pattern would have favoured the
460 upwelling of nutrient rich deep waters in the Antarctic sector of the Southern Ocean,as
461 inferred from marine sedimentary records (Anderson et al., 2009; Jaccard et al., 2013). The
462 nutrient and carbon laden southern waters would also have advected northward, via
463 Subantarctic Mode Water (Spero and Lea, 2002), and upwelled at the EEP providing extra
464 nutrients to the equatorial thermocline, promoting primary production during the last
465 deglaciation and possibly at older terminations (Winckler et al., 2016). The effective
466 transfer of nutrients northwards is also conditioned by nutrient utilization in the Southern
467 Ocean. Low nutrient utilization in the Antarctic Sector during deglaciations, caused by low
468 iron fluxes to the Southern Ocean (Jaccard et al., 2013), implies a large proportion of
469 nutrients being transported to low latitudes. The discussed ocean and atmospheric
470 teleconnections set a favourable scenario for an active connection between Southern Ocean
471 and Equatorial waters during deglacial periods as suggested by other authors for the last
472 two glacial cycles (Rippert et al., 2017). The correspondence between the peaks in
473 productivity during glacial terminations at thecore site and the abrupt rise in productivity in

474 the Antarctic sector of the Southern Ocean (ODP 1094, Ba/Fe, Jaccard et al., 2013)
475 suggests an intensification of the ocean tunnelling and an additional supply of nutrients
476 from the Southern Ocean to the U1381C site. This supply of nutrients could have
477 contributed to the increase in the productivity occurring at terminations in the easternmost
478 part of the EEP.
479 The data and interpretation discussed in this study provide a strong case for the
480 contribution of the EEP to the regulation ofpast ocean-atmosphere exchange of CO_2. The
481 intensification of the ocean tunnelling during terminations, evidenced by interhemispheric
482 productivity patterns, would have brought up CO_2 rich waters to the surface of the EEP
483 potentially contributing to the increase of the CO_2 atmospheric pool (e.g., Martinez-Boti et
484 al., 2015). However, a portion of this carbon would be taken up and exported by the
485 biological pump at the EEP, counterbalancing this oceanic CO_2 outgassing by transferring
486 carbon to the EEP interior. Although the net ocean-atmosphere flux at the tropical Pacific
487 over Middle to Late Pleistocene is yet unknown, the increase of productivity at
488 terminations might have acted to dampen the global atmospheric CO_2 increase occurring at
489 terminations (Bereiter et al., 2015). The described pattern might be applicable to other
490 tropical areas where the injection of southern sourced nutrients to low latitude Atlantic has
491 been interpreted to increase the productivity during the last deglaciation (Poggemann et al.,
492 2017).
493
494 **6.-Conclusions**
495 In this study, we obtained a multiproxy data set of independent proxies (geochemical,
496 micropaleoecological, sedimentological) that provide progress in our understanding of the
497 mechanisms promoting productivity changes within the easternmost part of EEP region.
498 We infer that the main processes promoting the increase of productivity in the EEP at

major and extra terminations over the last 650 ka is the shift of the ITCZ to a more southerly position (increased influence of the high productivity upwelling centre of the CRD) together with additional nutrient dvection from the Southern Ocean. From these arguments we infer that both interhemispheric oceanic and atmospheric mechanisms were involved in the productivity increase at terminations at the EEP. This deglacial productivity increase potentially played a role in the glacial-interglacial atmospheric CO_2 regulation by dampening the deglacial rise in atmospheric CO_2. The new data presented here suggest that the EEP is a key region in climate regulation playing a role in the global atmospheric and ocean reorganizations occurring at Middle to Late Pleistocene terminations.

Data availability: Data presented in this manuscript are provided in an excel file, Data.xls.

Acknowledgments

Authors would like to thank IODP for providing the sample material used to carry out this work and also the curators of the Green Coast Repository. This manuscript benefited from discussion and valuable comments from Samuel Jaccard (University of Bern). Comments and suggestions of two anonymous reviewers contributed to the improvement of the manuscript We acknowledge financial support from the Xunta de Galicia through a Project grant EM2013/012. This study is a contribution to the project CGL2016-7987R. P.D. was funded by a Contrato Parga Pondal and Investigador Distinguido UVIGO. P.B was supported by a Contrato Juan de la Cierva (JC1-2011-08849). I.H.A was funded by Swiss National Science Foundation Advanced Postdoc Mobility Grant (P300P2_164634). Authors appreciated the technical assistance of Rita González Villanueva.

References:

Anderson, R.F., Ali, S., Bradtmiller, L.I., Nielsen, S.H.H., Fleisher, M.Q., Anderson, B.E., Burckle, L.H., 2009. Wind-Driven Upwelling in the Southern Ocean and the Deglacial Rise in Atmospheric CO_2. Science 323, 1443-1448.

Barker, S., Chen, J., Gong, X., Jonkers, L., Knorr, G., Thornalley, D., 2015. Icebergs not the trigger for North Atlantic cold events. Nature 520, 333-336.

Bereiter, B., Eggleston, S., Schmitt, J., Nehrbass-Ahles, C., Stocker, T.F., Fischer, H., Kipfstuhl, S., Chappellaz, J., 2015. Revision of the EPICA Dome C CO2 record from 800 to 600 kyr before present. Geophysical Research Letters 42, 542-549.

Betancur, M.J., Martinez, I., 2003. Foraminíferos bentónicos recientes en sedimentos de fondo de la Cuenca de Panamá (Pacífico Colombiano), como indicadores de productividad y oxigenación. Boletín de Investigaciones Marinas y Costeras 32, 93-123.

Ceppi, P., Hwang, Y.-T., Liu, X., Frierson, D.M.W., Hartmann, D.L., 2013. The relationship between the ITCZ and the Southern Hemispheric eddy-driven jet. Journal of Geophysical Research: Atmospheres 118, 5136-5146.

Cheng, H., Edwards, R.L., Sinha, A., Spötl, C., Yi, L., Chen, S., Kelly, M., Kathayat, G., Wang, X., Li, X., Kong, X., Wang, Y., Ning, Y., Zhang, H., 2016. The Asian monsoon over the past 640,000 years and ice age terminations. Nature 534, 640-646.

Chiang, J.C.H., Lee, S.-Y., Putnam, A.E., Wang, X., 2014. South Pacific Split Jet, ITCZ shifts, and atmospheric North–South linkages during abrupt climate changes of the last glacial period. Earth and Planetary Science Letters 406, 233-246.

Denton, G.H., Anderson, R.F., Toggweiler, J.R., Edwards, R.L., Schaefer, J.M., Putnam, A.E., 2010. The Last Glacial Termination. Science 328, 1652-1656.

Fiedler, P.C., 2002. The annual cycle and biological effects of the Costa Rica Dome. Deep Sea Research Part I: Oceanographic Research Papers 49, 321-338.

Fiedler, P.C., Talley, L.D., 2006. Hydrography of the eastern tropical Pacific: A review. Progress in Oceanography 69, 143-180.

Goineau, A., Fontanier, C., Jorissen, F.J., Lansard, B., Buscail, R., Mouret, A., Kerhervé, P., Zaragosi, S., Ernoult, E., Artéro, C., Anschutz, P., Metzger, E., Rabouille, C., 2011. Live (stained) benthic foraminifera from the Rhône prodelta (Gulf of Lion, NW Mediterranean): Environmental controls on a river-dominated shelf. Journal of Sea Research 65, 58-75.

Gooday, A.J., 2003. Benthic foraminifera (protista) as tools in deep-water palaeoceanography: Environmental influences on faunal characteristics, Advances in Marine Biology. Academic Press, pp. 1-90.

Harris, R.N., Sakaguchi, A., Petronotis, K., Expedition 344 Scientists, 2013. Input Site U1381. Proceedings of the Integrated Ocean Drilling Program Volume 344 doi:10.2204/iodp.proc.344.103.2013.

Heinz, P., Ruschmeier, W., Hemleben, C., 2008. Live benthic foraminiferal assemblages at the Pacific continental margin of Costa Rica and Nicaragua. The Journal of Foraminiferal Research 38, 215.

Hofmann, E.E., Busalacchi, A.J., Q'Brien, J.J., 1981. Wind Generation of the Costa Rica Dome. Science 214, 552-554.

Ivanova, E.V., Beaufort, L., Vidal, L., Kucera, M., 2012. Precession forcing of productivity in the Eastern Equatorial Pacific during the last glacial cycle. Quaternary Science Reviews 40, 64-77.

Jaccard, S.L., Hayes, C.T., Martínez-García, A., Hodell, D.A., Anderson, R.F., Sigman, D.M., Haug, G.H., 2013. Two Modes of Change in Southern Ocean Productivity Over the Past Million Years. Science 339, 1419-1423.

Jacobel, A.W., McManus, J.F., Anderson, R.F., Winckler, G., 2016. Large deglacial shifts of the Pacific Intertropical Convergence Zone. Nature Communications 7, 10449.

Kienast, S.S., Kienast, M., Mix, A.C., Calvert, S.E., François, R., 2007. Thorium-230 normalized particle flux and sediment focusing in the Panama Basin region during the last 30,000 years. Paleoceanography 22, PA2213.

Krause, J.W., Stukel, M.R., Taylor, A.G., Taniguchi, D.A.A., De Verneil, A., Landry, M.R., 2016. Net biogenic silica production and the contribution of diatoms to new production and organic matter export in the Costa Rica Dome ecosystem. Journal of Plankton Research 38, 216-229.

LaMontagne, R.W., Murray, R.W., Wei, K.Y., Leinen, M., Wang, C.H., 1996. Decoupling of Carbonate Preservation, Carbonate Concentration, and Biogenic Accumulation: A 400-kyr Record from the Central Equatorial Pacific Ocean. Paleoceanography 11, 553-562.

Licari, L., Mackensen, A., 2005. Benthic foraminifera off West Africa (1ºN to 32ºS): Do live assemblages from the topmost sediment reliably record environmental variability? Marine Micropaleontology 55, 205-233.

Lisiecki, L.E., Raymo, M.E., 2005. A Pliocene-Pleistocene stack of 57 globally distributed benthic δ18O records. Paleoceanography 20, PA1003.

Locarnini, R.A., Mishonov, A.V., Antonov, J.I., Boyer, T.P., Garcia, H.E., Baranova, O.K., Zweng, M.M., Paver, C.R., Reagan, J.R., Johnson, D., Hamilton, R.M., Seidov, D., 2013. World Ocean Atlas 2013, Volume 1: Temperature, in: Levitus, S. (Ed.). Mishonov Technical Ed NOAA Atlas NESDIS 73, p. 40.

López-Otálvaro, G.-E., Flores, J.-A., Sierro, F.J., Cacho, I., 2008. Variations in coccolithophorid production in the Eastern Equatorial Pacific at ODP Site 1240 over the last seven glacial–interglacial cycles. Marine Micropaleontology 69, 52-69.

Lyle, M., Mix, A., Pisias, N., 2002. Patterns of CaCO3 deposition in the eastern tropical Pacific Ocean for the last 150 kyr: Evidence for a southeast Pacific depositional spike during marine isotope stage (MIS) 2. Paleoceanography 17, doi: 10.1029/2000PA000538.

Martinez-Boti, M.A., Marino, G., Foster, G.L., Ziveri, P., Henehan, M.J., Rae, J.W.B., Mortyn, P.G., Vance, D., 2015. Boron isotope evidence for oceanic carbon dioxide leakage during the last deglaciation. Nature 518, 219-222.

McManus, J.F., Oppo, D.W., Cullen, J.L., 1999. A 0.5-Million-Year Record of Millennial-Scale Climate Variability in the North Atlantic. Science 283, 971-975.

Meyers, P.A., 1997. Organic geochemical proxies of paleoceanographic, paleolimnologic, and paleoclimatic processes. Organic Geochemistry 27, 213-250.

Mojtahid, M., Griveaud, C., Fontanier, C., Anschutz, P., Jorissen, F.J., 2010. Live benthic foraminiferal faunas along a bathymetrical transect (140–4800 m) in the Bay of Biscay (NE Atlantic). Revue de Micropaléontologie 53, 139-162.

Morigi, C., Jorissen, F.J., Gervais, A., Guishard, S., Borsetti, A.M., 2001. Benthic foraminiferal faunas in surface sediments off NW Africa: Relationship with organic flux to the ocean floor. Journal of Foraminiferal Research 31, 350-368.

Mortlock, R.A., Froelich, P.N., 1989. A simple method for the rapid determination of biogenic opal in pelagic marine sediments. Deep Sea Research Part A. Oceanographic Research Papers 36, 1415-1426.

Murray, R.W., Leinen, M., Knowlton, C.W., 2012. Links between iron input and opal deposition in the Pleistocene equatorial Pacific Ocean. Nature Geoscience 5, 270-274.

Palter, J.B., Sarmiento, J.L., Gnanadesikan, A., Simeon, J., Slater, R.D., 2010. Fueling export production: nutrient return pathways from the deep ocean and their dependence on the Meridional Overturning Circulation. Biogeosciences 7, 3549-3568.

Pennington, J.T., Mahoney, K.L., Kuwahara, V.S., Kolber, D.D., Calienes, R., Chavez, F.P., 2006. Primary production in the eastern tropical Pacific: A review. Progress In Oceanography 69, 285-317.

Poggemann, D.-W., Hathorne, E.C., Nürnberg, D., Frank, M., Bruhn, I., Reißig, S., Bahr, A., 2017. Rapid deglacial injection of nutrients into the tropical Atlantic via Antarctic Intermediate Water. Earth and Planetary Science Letters 463, 118-126.

Ragueneau, O., Tréguer, P., Leynaert, A., Anderson, R.F., Brzezinski, M.A., DeMaster, D.J., Dugdale, R.C., Dymond, J., Fischer, G., François, R., Heinze, C., Maier-Reimer, E., Martin-Jézéquel, V., Nelson, D.M., Quéguiner, B., 2000. A review of the Si cycle in the modern ocean: recent progress and missing gaps in the application of biogenic opal as a paleoproductivity proxy. Global and Planetary Change 26, 317-365.

637 Reimer, P.J., Bard, E., Bayliss, A., Beck, J.W., Blackwell, P.G., Bronk Ramsey, C., Buck,
638 C.E., Cheng, H., Edwards, R.L., Friedrich, M., Grootes, P.M., Guilderson, T.P.,
639 Haflidason, H., Hajdas, I., Hatté, C., Heaton, T.J., Hoffmann, D.L., Hughen, K.A., Kaiser,
640 K.F., Kromer, B., Manning, S.W., Niu, M., Reimer, R.W., Richards, D.A., Scott, E.M.,
641 Southon, J.R., Staff, R.A., Turney, C.S.M., van der Plicht, J., Hogg, A., 2013. IntCal13 and
642 Marine13 radiocarbon age calibration curves 0-50,000 years cal BP. Radiocarbon 55,
643 1869-1887.

644 Rippert, N., Max, L., Mackensen, A., Cacho, I., Povea, P., Tiedemann, R., 2017.
645 Alternating Influence of Northern Versus Southern-Sourced Water Masses on the
646 Equatorial Pacific Subthermocline During the Past 240 ka. Paleoceanography 32, 1256-
647 1274.

648 Sarmiento, J.L., Gruber, N., Brzezinski, M.A., Dunne, J.P., 2003. High-latitude controls of
649 thermocline nutrients and low latitude biological productivity. Nature 427, 56-60.

650 Schneider, T., Bischoff, T., Haug, G.H., 2014. Migrations and dynamics of the
651 intertropical convergence zone. Nature 513, 45-53.

652 Sexton, P.F., Barker, S., 2012. Onset of 'Pacific-style' deep-sea sedimentary carbonate
653 cycles at the mid-Pleistocene transition. Earth and Planetary Science Letters 321-322, 81-
654 94.

655 Silva, K.A., Corliss, B.H., Rathburn, A.E., Thunell, R.C., 1996. Seasonality of living
656 benthic Foraminifera from the San Pedro Basin, California Borderland. The Journal of
657 Foraminiferal Research 26, 71-93.

658 Spero, H.J., Lea, D.W., 2002. The cause of Carbon Isotope Minimum Events on glacial
659 Terminations. Science 296, 522-525.

660 Stocker, T.F., Johnsen, S.J., 2003. A minimum thermodynamic model for the bipolar
661 seesaw. Paleoceanography 18, 1087.

662 Takahashi, T., Sutherland, S.C., Wanninkhof, R., Sweeney, C., Feely, R.A., Chipman,
663 D.W., Hales, B., Friederich, G., Chavez, F., Sabine, C., Watson, A., Bakker, D.C.E.,
664 Schuster, U., Metzl, N., Yoshikawa-Inoue, H., Ishii, M., Midorikawa, T., Nojiri, Y.,
665 Körtzinger, A., Steinhoff, T., Hoppema, M., Olafsson, J., Arnarson, T.S., Tilbrook, B.,
666 Johannessen, T., Olsen, A., Bellerby, R., Wong, C.S., Delille, B., Bates, N.R., de Baar,
667 H.J.W., 2009. Climatological mean and decadal change in surface ocean pCO2, and net
668 sea–air CO2 flux over the global oceans. Deep Sea Research Part II: Topical Studies in
669 Oceanography 56, 554-577.
670
671 Tetard, M., Licari, L., Beaufort, L., 2017. Oxygen history off Baja California over the last
672 80 kyr: A new foraminiferal-based record. Paleoceanography 32, 246-264.

673 Thunell, R.C., Keir, R.S., Honjo, S., 1981. Calcite Dissolution: An in situ Study in the
674 Panama Basin. Science 212, 659-661.

675 Tribovillard, N., Algeo, T.J., Lyons, T., Riboulleau, A., 2006. Trace metals as paleoredox
676 and paleoproductivity proxies: An update. Chemical Geology 232, 12-32.

Winckler, G., Anderson, R.F., Jaccard, S.L., Marcantonio, F., 2016. Ocean dynamics, not dust, have controlled equatorial Pacific productivity over the past 500,000 years. Proceedings of the National Academy of Sciences 113, 6119-6124.

Wright, A.K., Flower, B.P., 2002. Surface and deep ocean circulation in the subpolar North Atlantic during the mid-Pleistocene revolution. Paleoceanography 17, 20-21-20-16.

Yarincik, K.M., Murray, R.W., Peterson, L.C., 2000. Climatically sensitive eolian and hemipelagic deposition in the Cariaco Basin, Venezuela, over the past 578,000 years: Results from Al/Ti and K/Al. Paleoceanography 15, 210-228.

FIGURES AND FIGURE CAPTIONS

Figure 1: Location of Hole U1381C and regional hydrography

Figures on the left (a, b) represent the seasonal (winter above; summer below) depth (in meters below surface, mbs) of the 20°C isotherm in region of the EEP, which is used to identify the position of the Costa Rica Dome (Fiedler, 2002). The shadowed area represents the position of the ITCZ in winter (a) and summer (b). Thermocline temperature data are from World Ocean Database 2013 (Locarnini et al., 2013). The white circle indicates the location of Hole U1381C. Plots on the right (c, d) represents the winter (c) and summer (d) mean fields of SeaWiFS (September 1997 to July 2001) chlorophyll concentration in the region of the Costa Rica Dome. SeaWiFS data produced by NASA SeaWiFS Project and distributed by the Distributed Active Archive Center at NASA/Goddard Space Flight Center (http://oceancolor.gsfc.nasa.gov, accessed on 1st February 2018).

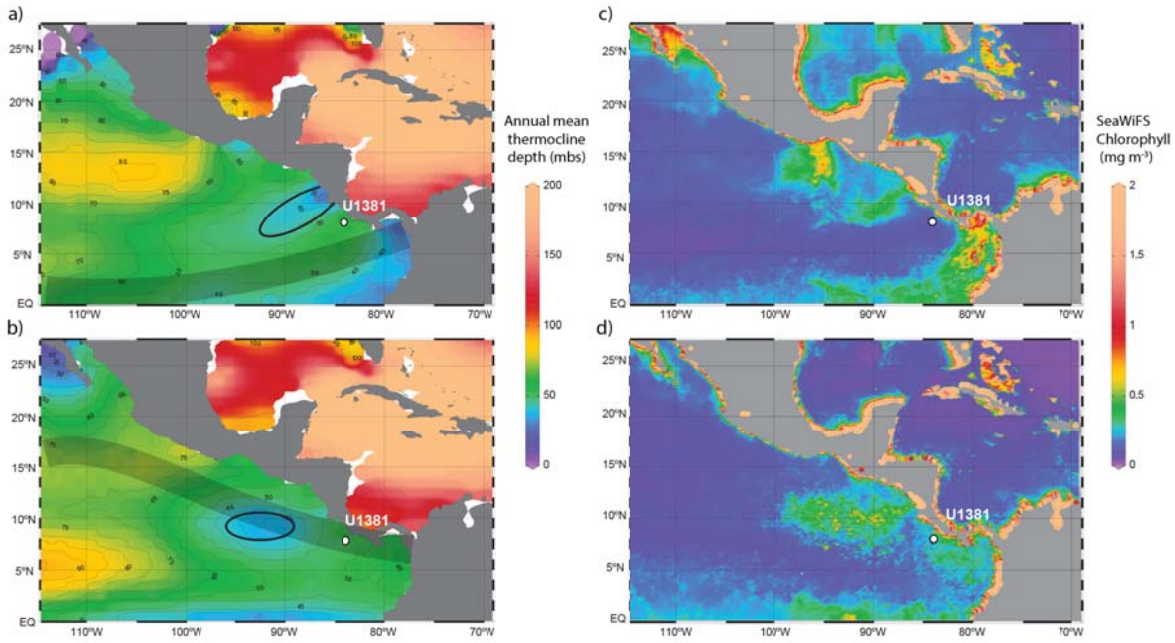

707

708 **Figure 2: Calcium carbonate variability.**

723 The benthic oxygen isotope record of *Uvigerina auberia*na (a) and carbonate records (b) of
724 Hole U1381C are compared with other proxies for carbonate dissolution/production
725 obtained in the same core (c-g). (b) % $CaCO_3$ and Ca/Ti (right axis) and mass $CaCO_3$
726 accumulation rate (left axis); (c) percent (right) and mass accumulation (left) of the coarse
727 fraction (%>63 µm); (d) abundance of benthic foraminifera (number of benthic
728 foraminifera >125 µm fraction per gram of dry weight sediment) and planktonic
729 foraminifera (number of planktonic foraminifera >150 µm fraction per gram of dry weight
730 sediment). The relation of benthic foraminifera to planktonic and benthic foraminifera
731 (B/P+B) is indicated in (e). The organic carbon content of the core is used as a proxy for
732 organic production (f) and complements the information provided by benthic foraminifera
733 (d). The opal content (%) is indicated in (g). Lines for the content of C_{org} (f) and %opal (g)
734 represent the 3-points running average. Vertical bars to the side of plots (f) and (g) indicate
735 standard error of C_{org} (±0.14%) and opal (±0.2%) analyses. Vertical grey bars indicate
736 glacial periods (light grey) and major terminations (dark grey) and "extra terminations"
737 (very dark grey). Brown vertical bars indicate potentially heavily dissolved intervals.

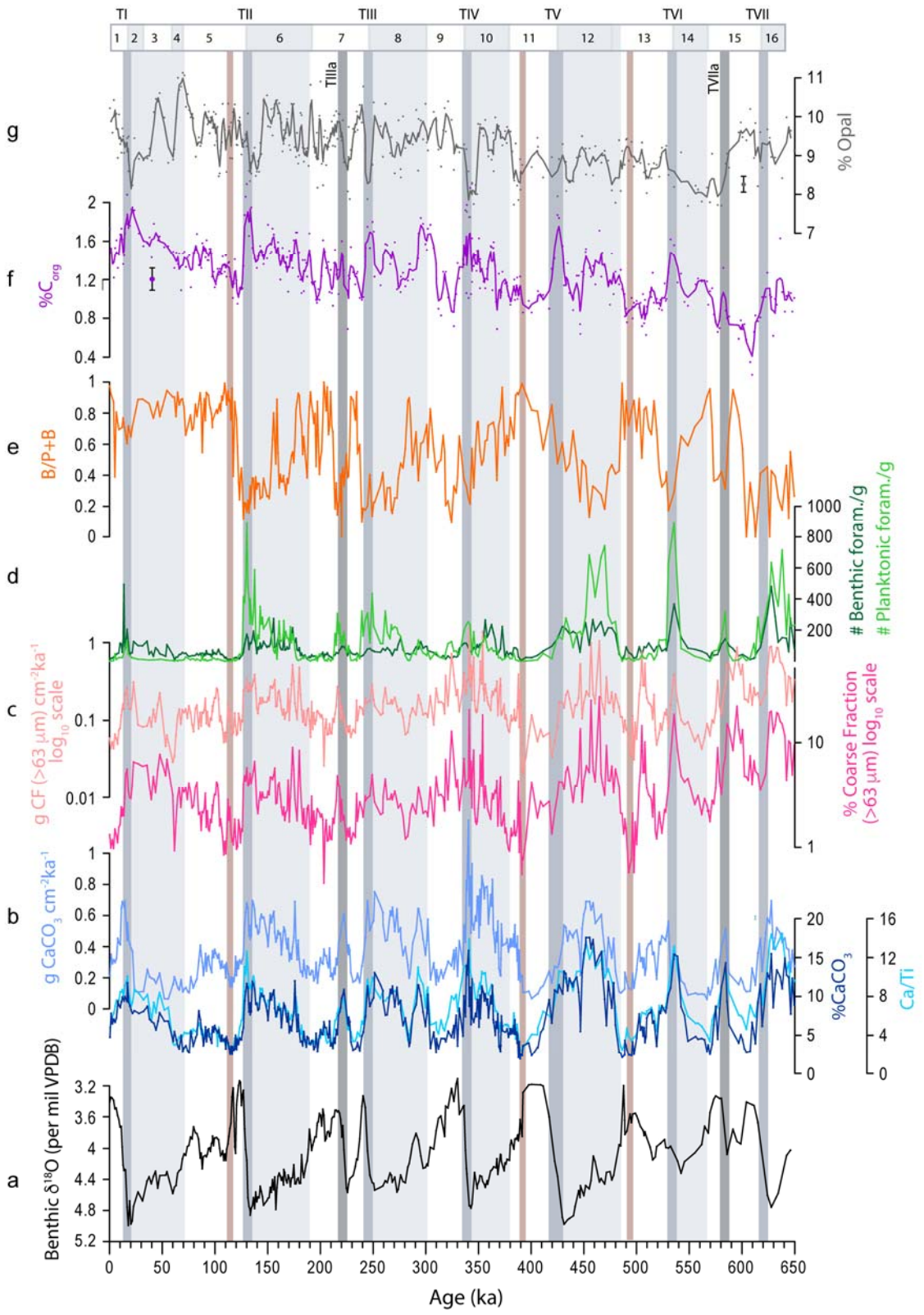

723

724 **Figure 3: Benthic foraminiferal assemblages**

725 The benthic $\delta^{18}O$ curve and the abundance of benthic foraminifera (number of benthic
726 foraminifera >125 μm per gram of dry weight sediment) are shown for reference in (a) and
727 (b). The records of the most characteristic species of benthic foraminifera in Hole U1381C
728 expressed in percentage are indicated in (c-f). Filled areas represent the 3-point running
729 average. The Si/C ratio (g, 3-point running average) is used here as a proxy for the
730 abundance of siliceous to non-siliceous primary producers. The Ti/Al record in the Hole
731 U1381C is plotted on inverted axis on the right (h) and the record of Ti/Al of ODP-1002
732 on the left (Yarincik et al., 2000) (i). The Ti/Al records indicate decreased (increased)
733 runoff - high (low) Ti/Al ratios- which are related to the relative movement of the
734 terrestrial ITCZ with high (low) ratios corresponding to a southerly (northerly)-most
735 position of the ITCZ. The average error of Ti/Al and Si/C measurements is indicated by
736 vertical bars to the side of plots (g) and (h). The *Uvigerina* spp. group includes *Uvigerina*
737 *auberiana* and *Uvigerina peregrina*. The group of the so called intermediate hypoxic
738 species includes *Bolivina interjuncta*, *Bolivina seminuda*, *Bolivina* cf. *plicata*,
739 *Epistominella pacifica* and *Epistominella smithi.* Vertical grey bars are as indicated in
740 Figure 2.

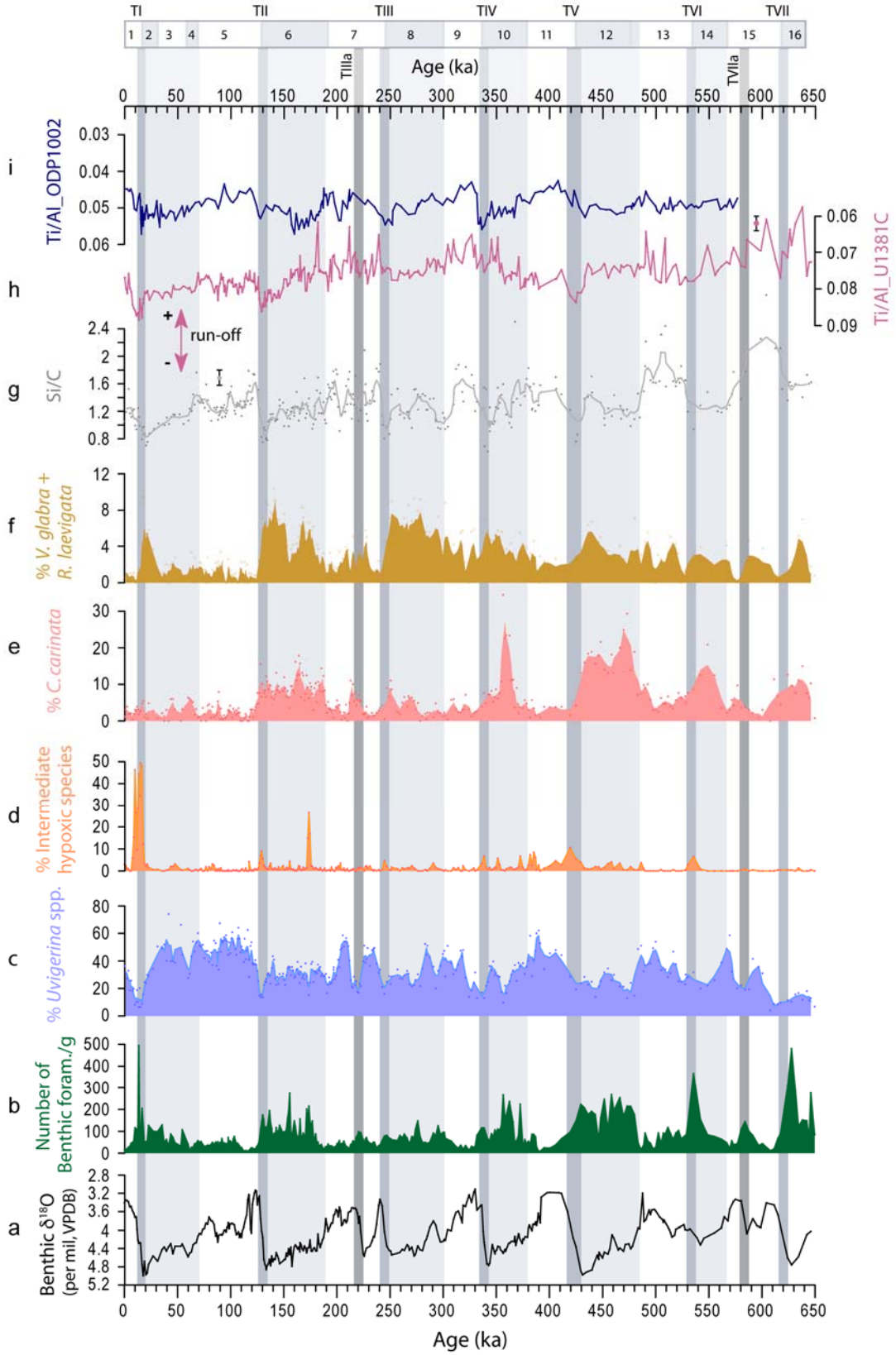
TI
TII
TIII
TIV
TV
TVI
TVII
1 2 3 4 5 6 7 8 9 10 11 12 13 14 15 16
TIIIa
TVIIa
Age (ka)
0 50 100 150 200 250 300 350 400 450 500 550 600 650
i
Ti/Al_ODP1002
0.03 0.04 0.05 0.06
h
Ti/Al_U1381C
0.06 0.07 0.08 0.09
run-off
+
-
g
Si/C
2.4 2 1.6 1.2 0.8
f
% V. glabra + R. laevigata
12 8 4 0
e
% C. carinata
30 20 10 0
d
% Intermediate hypoxic species
50 40 30 20 10 0
c
% Uvigerina spp.
80 60 40 20 0
b
Number of Benthic foram./g
500 400 300 200 100 0
a
Benthic δ18O (per mil, VPDB)
2.8 3.2 3.6 4 4.4 4.8 5.2
0 50 100 150 200 250 300 350 400 450 500 550 600 650
Age (ka)

741

742

743

Figure 4:Atmospheric and oceanic interplay at terminations.

Proxies for the Antarctic Continent (a), the Antarctic sector of the Southern Ocean (b) are compared to proxies obtained in the EEP (c-d; Hole U1381C, this study), central Asia (e) and the high latitude North Atlantic (f). The oxygen isotope record of Hole U1381C (a, grey) is plotted to the right of the Antarctic CO_2 composite (Bereiter et al., 2015). The productivity record of the Antarctic sector of the Southern Ocean (b) is represented by the Ba/Fe record of ODP Site 1094 (Jaccard et al., 2013) and is compared to Hole U1381C records of (c) $\%C_{org}$ as a proxy for productivity and (d) the percentage of *Uvigerina* spp. group, which is related to the influence of the Costa Rica Dome and therefore, a proxy for the relative position of the ITCZ. The increased (decreased) abundance of *Uvigerina* spp. is related to the northward (southward) position of the ITCZ. Data from this study lead to the suggestion that the southernmost position of the ITCZ in the EEP is attained at terminations (both major and extra terminations) in close correspondence with abrupt weakening of the Asian Monsoon (e). The record of $\Delta\delta^{18}O$ (e) from Chinese caves represents a cave composite $\delta^{18}O$ signal obtained after removing the orbital insolation component (Cheng et al., 2016). Records of Ice Rafted Detritus (IRD, number/g) in the high latitude North Atlantic (ODP Site 983 data from Barker et al., 2015, redline; ODP Site 980 data from McManus et al., 1999 and Wright and Flower, 2002, orange line) are indicated in (f). Note that age models are plotted on their published age scales; ODP Sites 983 and 1094 are tuned to ice core records whereas Hole U1381C and ODP Site 980 are tuned to an orbital stack. Vertical bars are as indicated in Figure 2.

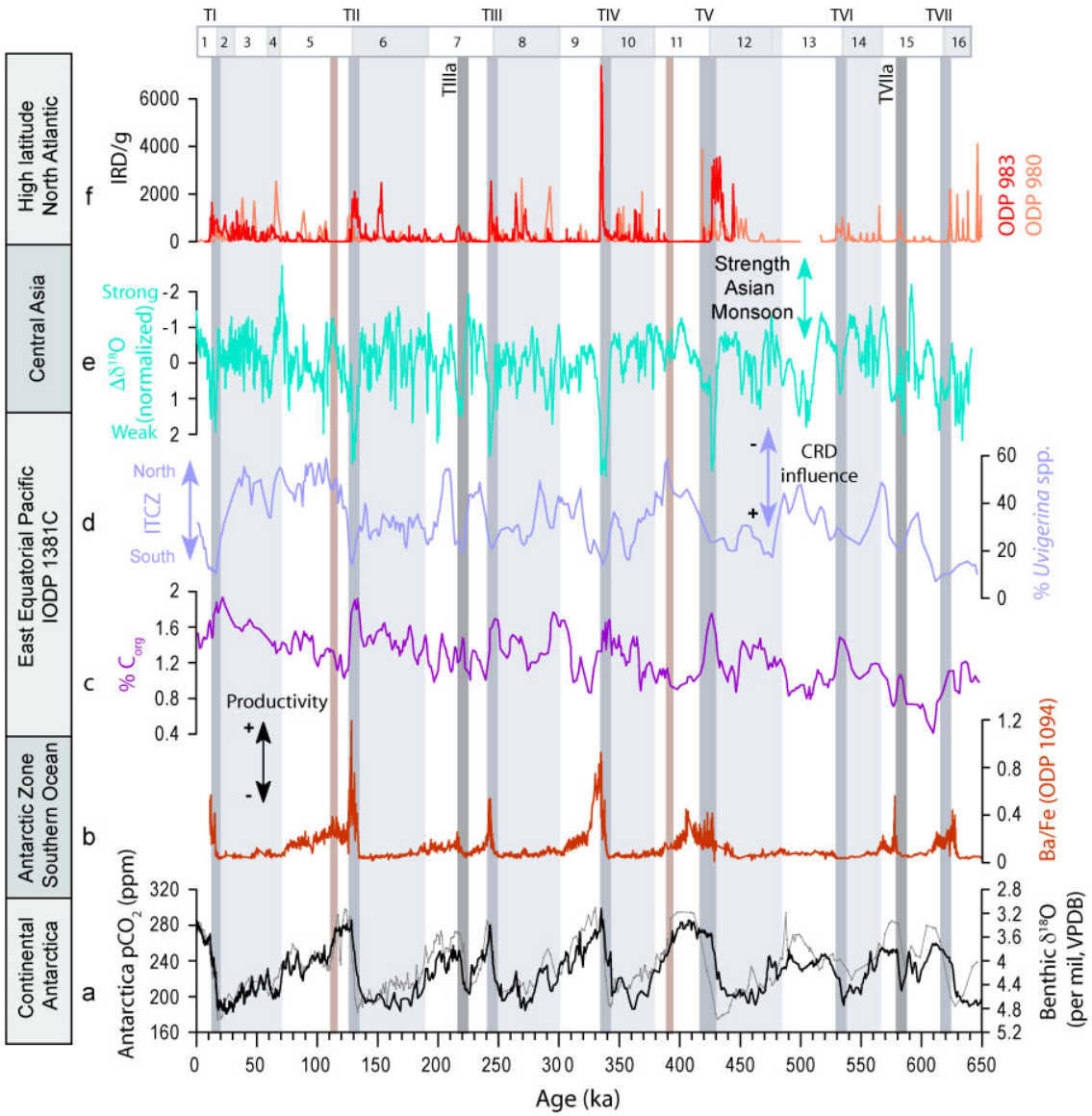

765

766

767

768

769

770

771

772

773